JOURNAL OF CATALYSIS 149, 449–457 (1994)

Characterization of Catalytically Active Sites on Aluminum Oxides, Hydroxyfluorides, and Fluorides in Correlation with Their Catalytic Behavior

A. Hess and E. Kemnitz

Fachbereich Chemie, Humboldt-Universität zu Berlin, Hessische Strasse 1/2, D-10115 Berlin, Germany

Received June 9, 1993; revised February 23, 1994

Temperature-programmed desorption of ammonia has been employed for the characterization of halogen exchange catalysts. Non-activated and activated catalysts are compared in regard to their behavior in adsorption and desorption. Activation of γ-alumina and $AlF_3(OH)$ increases both the catalytic activity for halogen exchange and the amount and strength of ammonia adsorption. In constrast, β-AlF_3 possesses catalytic activity already without activation. This substance reveals no significant alteration of ammonia adsorption after activation. A connection was observed between the acidity of the catalysts and their reactivity. The nature of the acidic sites was determined by Fourier transform infrared photoacoustic spectroscopy of pyridine chemisorbed on the solid surfaces. The results indicate that Lewis acid sites of a certain strength are responsible for the catalytic activity. © 1994 Academic Press, Inc.

INTRODUCTION

Halogen exchange reactions are widely used, e.g., for the synthesis of fluorocarbons. One of the technical routes is vapor-phase fluorination of chlorocarbons with HF over fluorinated metal oxide catalysts. The dismutation reaction is one of the side reactions observed in this system. All these halogen exchange reactions proceed only in the presence of a catalyst. Heterogeneously catalyzed halogen exchange reactions normally require preactivation of the catalysts. In the case of aluminum or chromium oxides a haloalkane flow is often applied for catalyst activation.

Recently, we have published an ESCA and XRD study on these activation processes (1) and we made suggestions about the reactions occurring during the activation (2). The present work continues this study with regard to characterization of the acidic properties of the solid samples before and after activation procedures. Temperature-programmed desorption (TPD) of ammonia (a basic probe molecule) was employed.

Peri (3) and many others [e.g., (4, 5)] have investigated the interaction of ammonia with γ-alumina using infrared spectroscopy. Most of the ammonia is adsorbed molecularly on Lewis acid aluminum cations. NH_4^+ (ammonia adsorbed on Brønsted acid Al–OH sites) could not be observed, but this may depend on the origin of the sample (calcination procedure). However, it can be assumed that the TPD intensities (magnitudes of the TPD profiles) of desorbed ammonia represent the amounts of both Lewis and Brønsted acid sites.

In the case of chlorinated alumina an even more difficult behavior is observed. Here, NH_2^- can replace Cl^- ions. Therefore, the correlation between ammonia adsorption and acidity is slightly ambiguous. Concerning our alumina samples, we can state that they contain traces of chloride only after activation. Instead, considerable F uptake is observed. Peri (6) also investigated the effect of fluoride on the surface acid sites of γ-alumina. IR studies of CO_2 and CO adsorption show that fluoride strengthens certain Lewis acid sites (α sites). CO_2 is held more strongly and exhibits higher IR frequencies compared with unmodified γ-alumina. The complete replacement of OH by F removes the Brønsted acidity and eliminates *M*–O–*M* linkages. The strengthening of these sites is assumed to be responsible for an increase in the polymerization activity of fluorinated alumina (6).

Since TPD of ammonia is influenced by both Lewis and Brønsted acidity it is necessary to distinguish between these types of acid sites. Usually, the infrared spectra of the chemisorbed ammonia reveal this information. On our samples we have observed a large broadening of the characteristic infrared bands, probably due to the large amount of OH groups in our samples. Therefore, we have changed to a different probe molecule. The use of pyridine to determine the nature of acidity on solid surfaces has been well established (7–14).

The lone-pair electron of the nitrogen atom of pyridine can either bind coordinately to *Lewis acid sites* (*"LPy"*) or interact with acidic OH gruops to form pyridinium cations or pyridine adsorbed via hydrogen bridge bonds (*Brønsted sites, "BPy"*). The 19b and 8a ring vibration

0021-9517/94 $6.00

TABLE 1

Characteristic Infrared Bands of Pyridine Chemisorbed on γ-Alumina and Their Interpretations

Band (cm^{-1})	Interpretation	Reference
1261	Possibly N=O vibration of pyridine N-oxide	(13)
1435	19b pyridine, gaseous, 20°C, (very strong)	This work
1438	19b pyridine, liquid, 20°C, (very strong)	This work
1445–1455	19b pyridine coordinately bonded to Lewis acid sites (LPy)	(7, 9, 12, 13), this work
1449	19b pyridine, gaseous, 20°C (very strong)	This work
1482	19a pyridine, liquid, 20°C (medium)	This work
1492	19a pyridine, gaseous, 20°C (weak)	This work
1493	19a pyridine coordinately bonded to Lewis acid sites (LPy)	(7, 12), this work
	19a pyridine bonded to Brønsted acid sites (BPy)	(7), this work
1540–1550	19b pyridine hydrogen bonded to quasi-Brønsted acid site (BPy)	(7, 8, 12), this work
1570	8b pyridine, gaseous and liquid, 20°C (medium)	This work
1578	8b pyridine coordinately bonded to Lewis acid sites (LPy)	(7, 12), this work
1580	Possibly N–H deformation mode of Py–H$^+$	(13)
1581	8a pyridine, liquid, 20°C (very strong)	This work
1586	8a pyridine, gaseous, 20°C (very strong)	This work
1590	8a pyridine hydrogen bonded to quasi-Brønsted acid sites (BPy)	(10, 11)
	8a pyridine coordinately bonded to octahedral aluminum Lewis acid sites (LPy)	(11), this work
1595	8a pyridine coordinately bonded to octahedral aluminum Lewis acid sites (calcination temperatures >650 K) (LPy)	(11), this work
1598	Pyridine, liquid, 20°C, combination mode (medium)	This work
~1615	8a pyridine, coordinately bonded to Lewis acid sites of lower strength (LPy), (11) assigned them to tetrahedral aluminum vacancies	(7, 9, 11, 12), this work
~1620	8a pyridine coordinately bonded to Lewis acid sites of higher strength (LPy), (11) assigned them to tetrahedral aluminum vacancies	(7, 9, 11, 12), this work
1634	Possibly pyridone C=O mode	(8)
1639	8a Py–H$^+$ pyridinium cation (BPy)	(7, 8, 12), this work
2450	Possibly N–H stretching vibration of Py–H$^+$	(13)

modes of the pyridine molecule (15) are very sensitive for distinguishing between adsorption on Lewis sites and that on Brønsted acid sites. Table 1 summarizes knowledge on the characteristic infrared bands of pyridine chemisorbed on γ-Al_2O_3 and their assignments.

Matulewicz *et al.* (14) characterized fluorinated alumina (treatment with gaseous NH_4F or aqueous impregnation with NH_4F) by poisoning using pyridine and some of its derivatives (e.g., 2,6-dimethylpyridine). By use of pyridine as an adsorbate on fluorinated alumina, only Lewis acid sites were determined, although pyridine is sensitive to both Lewis and Brønsted acid sites. If 2,6-dimethylpyridine is used then some Brønsted sites become visible. This can be explained by the higher basicity of the latter molecule, leading to an interaction with even very weak Brønsted acid sites.

In some cases, conversion of Lewis into Brønsted sites has been observed after addition of water. Kerkhof *et al.* (16) reported a correlation between the presence of Brønsted acid sites on fluorinated alumina and its catalytic activity for the oligomerization of 2-methylpropene. They used 2,6-dimethylpyridine as a specific poison for Brønsted acid sites on fluorinated alumina.

We have used pyridine for the identification of the sites since it does not show a steric hindrance to Lewis (or Brønsted) sites like 2,6-dimethylpyridine. Although the basicity and the molecular diameter of ammonia (used for TPD) and pyridine are different, combination of these methods permits good characterization of the acid sites on the surfaces of our catalysts.

Ammonia thermodesorption experiments and infrared measurements of the pyridine adsorption complexes are compared with the catalytic activity of the respective solid sample for halogen exchange. The dismutation reaction of $CHClF_2$ (17) is used as a model reaction for halogen exchange:

$$2CHClF_2 \rightleftharpoons CHF_3 + CHCl_2F \quad (1)$$

$$2CHCl_2F \rightleftharpoons CHClF_2 + CHCl_3 \quad (2)$$

EXPERIMENTAL

Temperature-Programmed Desorption

Seven-tenths gram of the solid sample was used in a flow reactor (platinum, constant carrier gas flow of 0.5 liter/h dried nitrogen during the measurement). The starting substances were dried in the same way as was done before the activation. Afterward, TPD without feed of probe molecules (only nitrogen flow) was carried out. The same TPD procedure was employed with the activated samples (degasification products were detected). After this preparation a pulse of 1, 5, 18, or 30 ml of the probe molecule was fed (using a six-port valve) at 100°C. This pulse was streamed through PTFE tubing into the reactor and, after leaving the reactor, into a PTFE flow cell (10 cm long, KBr windows), where its concentration was determined with a a Perkin–Elmer FTIR spectrometer System 2000. The computer program TRIR (Perkin–Elmer) was employed to create the desorption profiles from the IR data. The concentration of ammonia was followed in the region 932–928 cm^{-1}, that of HCl at 2825–2815 cm^{-1}, that of water at 1590–1490 cm^{-1}, and that of HF at 4080–4070 cm^{-1}. The extinction coefficients were determined by calibration under the same flow conditions. The experimental error regarding the amounts of desorbed substance did not exceed ±5%.

The following temperature programs were employed (Honeywell temperature control unit, ±0.15% deviation from set point):

γ-Al_2O_3, α-AlF_3 and α-Cr_2O_3: after the feed pulse, 10 min isothermal 100°C, then 7.5 K/min up to 700°C, total run time 90 min.

β-AlF_3: after the feed pulse, 5 min isothermal 100°C, then 7.5 K/min up to 475°C (structure would be destroyed at higher temperatures), total run time 55 min.

$AlF_2(OH)$: after the feed pulse, 5 min isothermal 100°C, then 7.5 K/min up to 400°C (structure would be destroyed at higher temperatures), total run time 45 min.

Ammonia was used as a basic probe molecule to interact with both Lewis and Brønsted sites. Ammonium fluoride may be formed on the surface of fluoride-containing samples. Sublimed ammonium fluoride in other parts of the reactor was not observed.

Infrared Photoacoustic Spectroscopy of Chemisorbed Pyridine

One hundred milligrams of the solid sample was used in a flow reactor similar to the one used for TPD measurements. During the experiment a constant flow of 0.5 liter/h dried nitrogen was employed. The pyridine feed was carried out in the following way. Thirty microliters of liquid pyridine was injected into a vaporizer (150°C) located just before the inlet of the flow reactor. The excess gaseous and physisorbed pyridine was removed by holding the temperature for 15 min under the controlled nitrogen flow. After it was cooled, the sample was transferred into the sample holder of the photoacoustic cell (MTEC in connection with FTIR Perkin–Elmer System 2000). The sample was purged for 10 min with dried helium. Then 64 or more scans were taken (resolution 8 or 4 cm^{-1}).

The framework vibrations of the solid sample were used as an internal reference standard. All figures show normalized photoacoustic (PA) spectra.

Activation of Catalysts

Detailed information about the synthesis of the solid samples is available in Ref. (1). Here, the specific surface areas (BET) are presented:

γ-Al_2O_3: dried—210 m^2/g, activated—160 m^2/g
α-Cr_2O_3: dried—70 m^2/g, activated—;68 m^2/g
β-AlF_3: both dried and activated—31 m^2/g
$AlF_2(OH)$: both dried and activated—15 m^2/g
α-AlF_3: 1 m^2/g (higher weights were used to increase the absolute surface area)

The activation was carried out in the following way:

γ-Al_2O_3-250 and α-Cr_2O_3-250: dried under N_2 flow (250°C, 30 min), subsequently treated with $CHClF_2$ (3 liters/h, 250°C, 30 min), degasification under N_2 flow (250°C, 15 min)

γ-Al_2O_3-400 and α-Cr_2O_3-400: dried under N_2 flow (250°C, 30 min), subsequently treated with $CHClF_2$ (3 liters/h, 400°C, 30 min), degasification under N_2 flow (400°C, 15 min)

β-AlF_3-350: dried under N_2 flow (20–350°C, 20 K/min, 20 min 350°C), subsequently treated with $CHClF_2$ (3 liters/h, 350°C, 30 min), degasification under N_2 flow (350°C, 15 min)

$Alf_2(OH)$-350: dried under N_2 flow (20–350°C, 20 K/min, 20 min 350°C), subsequently treated with $CHClF_2$ (3 liters/h, 350°C, 30 min), degasification under N_2 flow (350°C, 15 min)

After activation, TPD measurements of the samples were carried out. The use of platinum tube reactors with stopcocks on their ends permitted the sample transfer without contact with air and moisture. Nevertheless, during transfer of sample from the pyridine feed reactor to the PA cell, a short air contact could not be prevented since working in the glove box with the highly sensitive microphone membrane of the PA cell is not possible.

For the changes in the concentrations during the activation and the changes in the solid samples we refer to Ref. (1).

Determination of Reactivity of the Catalysts

A constant bulk volume of 0.062 ml (determined with bulk density and weight) of the activated catalyst was used in a flow reactor. A constant $CHClF_2$ flow (3 liters/h) was adjusted. The composition of the gas phase at the exist of the reactor was determined by gas chromatography (used column: Poraplot u, i.d. 0.53 mm, length 25 m). The conversion of the starting substance was determined at different temperatures. Equal bulk volumes and equal flows results in approximately equal residence time. Therefore, the conversions of different samples are comparable. Specific reactivity $r_s = r/s$ (rate divided by surface area) was defined. The surface area was calculated using the weight and the specific surface area of the catalyst. The rate was determined by dividing the conversion of the starting substance $CHClF_2$ by the residence time (approximation of linear decrease of starting substance). Therefore, the value r_s represents an approximated specific reactivity of the catalyst.

RESULTS

Influence of Preexisting Hydroxyl Groups on TPD

Figure 1a shows ammonia TPD profiles ("spectra") of calcined, nonactivated γ-alumina. During the isothermal period the nonadsorbed breakthrough of ammonia can be seen. In the case of the 5-ml feed all ammonia is adsorbed.

It is noticeable that the first feed gives lower desorption intensities compared with the following ones. The reason is that preexisting water occupies the same sites as those preferred by ammonia. After the water is released (Fig. 1b), a larger amount of ammonia can be adsorbed and desorbed. Therefore, the second and third feeds look similar.

In the following TPD spectra the second feeds are compared to exclude the influence of preexisting water and OH groups.

Ammonia TPD and Pyridine Adsorption Complexes on Calcined and Activated Catalysts

γ-Alumina. Figure 2 presents the ammonia TPD profiles of calcined, low-temperature-activated and high-temperature-activated γ-alumina samples. As a result of activation with $CHClF_2$, the number and the strength of the acidic sites have dramatically increased. Obviously, this is due to the inductive effect of OH and O replacement by F occurring during the activation. The activated samples contain 7–13 wt% fluoride (amorphous) and only traces of chloride (<0.2 wt%). ESCA confirms partial F-for-OH and F-for-O exchanges (1). After activation the sample reveals catalytic activity for the dismutation of $CHClF_2$.

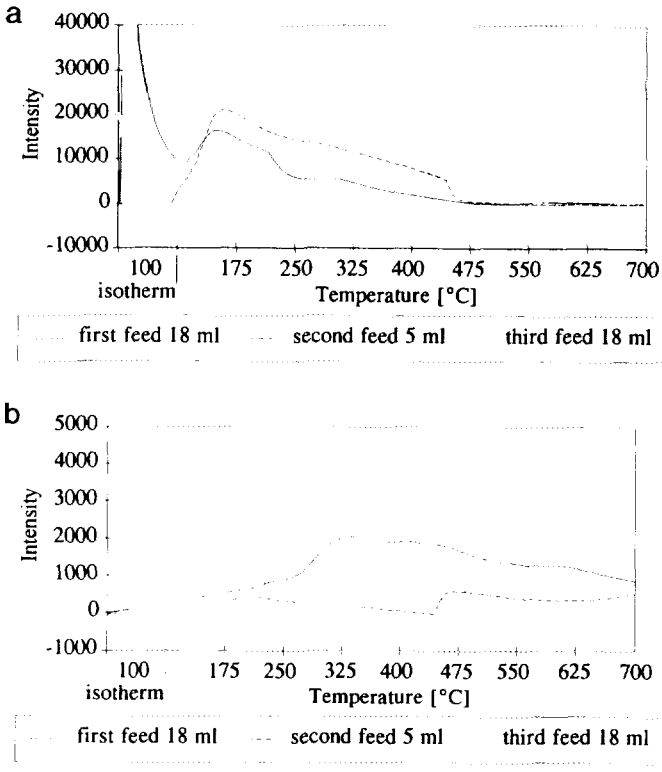

FIG. 1. Ammonia TPD profiles of γ-alumina calcined at 250°C: (a) desorbed ammonia, (b) released water.

Activation at 400°C results in a decrease in these sites. This can be explained by the enormous coke formation leading to deactivation of catalytically active sites. This deactivation seems to occur over the whole range of site strength, resulting in a lowering of desorption intensities along the entire temperature range. A respective decrease

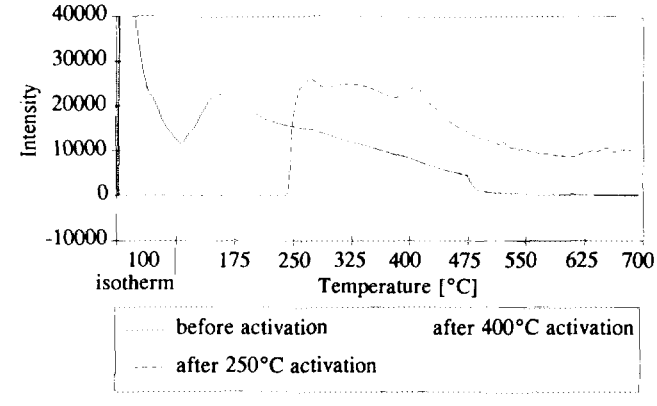

FIG. 2. Ammonia TPD profiles of calcined and activated γ-alumina samples (the respective 18-ml feed are compared).

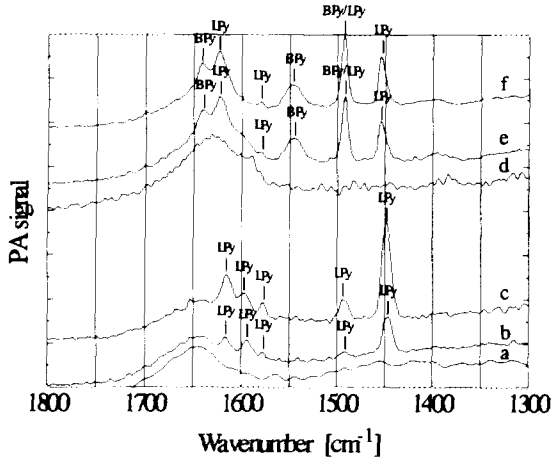

FIG. 3. FTIR photoacoustic spectra of pyridine chemisorbed on modified γ-alumina samples: (a) calcined (250°C) (background); (b) calcined (250°C), pyridine adsorption (150°C, 30 μl); (c) calcined (250–700°C), pyridine adsorption (150°C, 30 μl); (d) activated with $CHClF_2$ (250°C), calcined (250°C) (background); (e) activated with $CHClF_2$ (250°C), calcined (250°C), pyridine adsorption (150°C, 30 μl); (f) activated with $CHClF_2$ (250°C), calcined (250–700°C), pyridine adsorption (150°C, 30 μl) (pyridine chemisorbed on 400°C activated γ-alumina is similar to Fig. 3e).

in the catalytic activity due to coke formation was observed.

Figure 3 presents a comparison between the IR photoacoustic spectra of calcined and activated γ-alumina samples before and after the adsorption of 30 μl pyridine. After pyridine contact, the calcined sample (Fig. 3b) shows bands representing pyridine chemisorbed on Lewis acid sites (LPy). Brønsted sites are not present, a fact that is confirmed by many authors [e.g., (7, 14)]. Calcination of this sample up to 700°C results in an increase in the number of Lewis acid sites (see Fig. 3c), whereas Brønsted acid sites are not formed. This alteration can be compared with the increase in ammonia adsorption after the first temperature program (see Fig. 1), where the higher calcination temperature removes the adsorbed water. After that more Lewis sites can be entered by the probe molecules.

When the 250°C calcined sample (Fig. 3b) and the 250°C activated sample (Fig. 3e) are compared, remarkable alterations can be observed. The number of Lewis acid sites has not significantly increased, but from the 19b mode at approximately 1450 cm^{-1}, it can be seen that a shift to higher wavenumbers has occurred.

Morterra and Cerrato (10) have reported frequency shifts that arise from a change in pyridine coverage. An increase in pyridine coverage results in a shift to lower wavenumbers. Our activated sample offers a slightly higher degree of pyridine coverage compared with the calcined sample. Therefore, a shift downward should occur, but the opposite is observed. It can be concluded that the increase in strength of the Lewis acid sites is the reason for the observed shift to higher wavenumbers.

A further significant difference between the calcined and activated samples (Figs. 3b and 3e) is the formation of Brønsted acid sites (BPy). Pyridinium cations as well as H-bridge-bonded pyridine became visible. Since other samples like β-AlF_3 or activated α-Cr_2O_3 do not reveal Brønsted acid sites, but catalyze the dismutation model reaction very well, it can be assumed that Brønsted acid sites are not required for the catalytic activity. Figure 3f illustrates that a temperature program for an activated sample up to 700°C does not form new sites. Obviously, all surface water is removed by the activation process which previously blocked active sites (compare Fig. 3f wth Fig. 3c).

γ-Alumina that is activated at 400°C behaves similarly to the 250°C activated sample. On the other hand, the TPD profiles showed decreasing ammonia desorption intensities due to the higher extent of coke formation. Obviously, the behaviors of the probe molecules ammonia and pyridine are different, possibly due to the different diameters of the molecules.

α-Cr_2O_3. The behavior of α-Cr_2O_3 differs from that of γ-alumina (Fig. 4). There is only a slight increase in ammonia desorption intensities at higher temperatures after 250°C activation. Samples activated at 400°C exhibit lower degrees of coke formation compared with the respective γ-alumina samples. Therefore, the restricted desorption properties should be explained by coke formation and possibly by a thin product layer with a decreased amount of active sites [e.g., thermodynamically favored, but catalytically inactive $CrCl_3$ layer (18)].

The activated samples exhibit slight chloride uptakes (1–2 wt%) and very small fluoride uptakes (about 0.3 wt%).

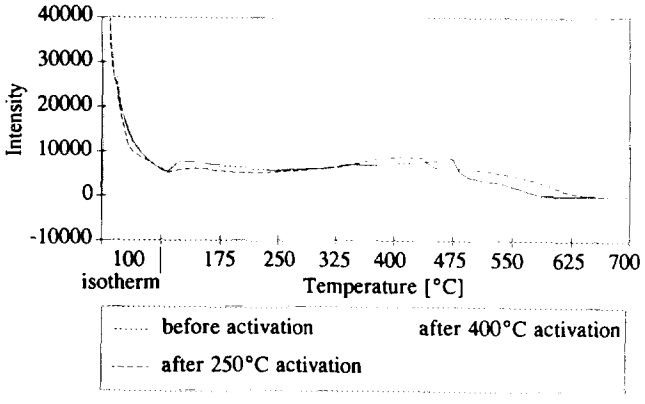

FIG. 4. Ammonia TPD profiles of calcined and activated α-Cr_2O_3 samples (the respective 5-ml feeds are compared).

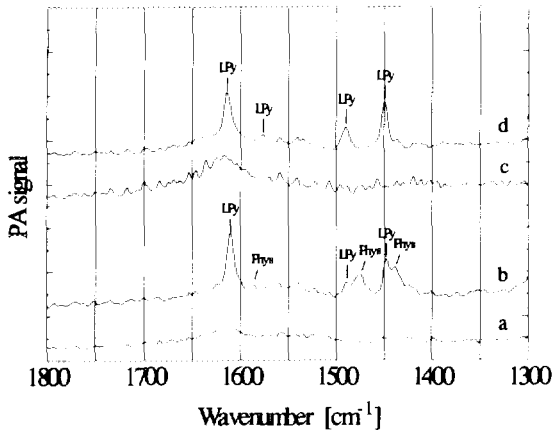

FIG. 5. FTIR photoacoustic spectra of pyridine chemisorbed on modified α-Cr_2O_3 samples: (a) calcined (250°C) (background); (b) calcined (250°C), pyridine adsorption (150°C, 30 μl); (c) activated with $CHClF_2$ (250°C), calcined (250°C) (background); (d) activated with $CHClF_2$ (250°C), calcined (250°C), pyridine adsorption (150°C, 30 μl).

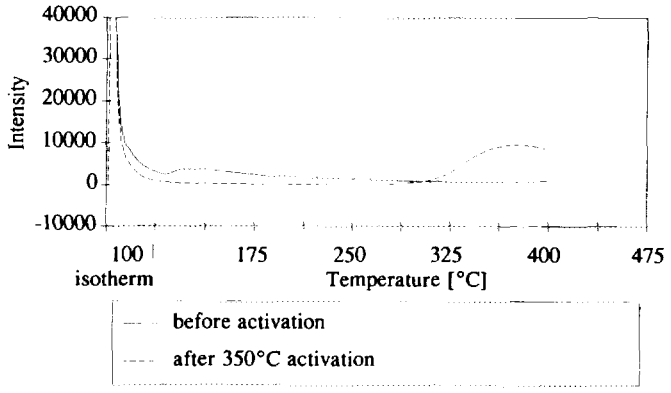

FIG. 6. Ammonia TPD profiles of calcined and activated $AlF_2(OH)$ (the respective 5-ml feeds are compared).

As can be seen from Fig. 5, the calcined sample offers Lewis acid sites and a few bands arising from physisorbed pyridine. After activation with $CHClF_2$ the sample reveals no significant alteration in the number of Lewis sites, but a small shift to higher wavenumbers, similar to the behavior of γ-alumina, can be observed. After activation the sample exhibits catalytic activity for the dismutation reaction.

Pyridine chemisorbed on Brønsted acid sites is not present. Therefore, it can be assumed that Brønsted acidity is not essential for the catalysis of the dismutation reaction.

$AlF_2(OH)$. As can be seen from Fig. 6, the activated sample desorbs considerably larger amounts of ammonia in the temperature region above 325°C. This is accompanied by reaching catalytic activity while the simply calcined sample does not exhibit any catalytic activity. According to ESCA a partial F-for-OH exchange of the activated sample has occurred (1). Unfortunately, measurement of chemisorbed pyridine is not possible, since this sample shows strong IR absorptions due to framework vibrations within the characteristic infrared region of chemisorbed pyridine.

β-AlF_3. According to Fig. 7 the nonactivated sample already possesses a large amount of strong sites, which is slightly decreased after activation. This is due to the observed coke formation. Other changes for the activated sample were not observed [XRD, IR, ESCA (1)]. Calcined β-AlF_3 already exhibits full catalytic activity. This sample is the only one that is catalytically active without any previous activation.

According to the observed catalytic behavior and the ammonia desorption profiles, the spectra of chemisorbed pyridine reveal no significant alterations between the calcined and the activated samples. As can be seen from Figs. 8b and d, both calcined and activated β-AlF_3 show the IR bands of pyridine chemisorbed on Lewis acid sites. Brønsted acid sites do not occur.

Figure 9 illustrates an ammonia TPD of a nonactivated sample up to 700°C, a temperature region that leads to reconstruction of the lattice forming α-AlF_3. The first feed exhibits the normal desorption behavior of β-AlF_3. The second feed characterizes the behavior of the product α-AlF_3. The active sites were destroyed. Furthermore, after this procedure the sample does not chemisorb pyridine at a detectable level. The IR bands of chemisorbed pyridine to not appear. The catalytic behavior of the high-temperature calcined sample is similar to the behavior of α-AlF_3, which is reported in the next paragraph.

α-AlF_3. Crystalline α-AlF_3 exhibits no adsorption and desorption of ammonia or pyridine. Only the introduction of crystal disorders or partial hydrolysis leads to a change

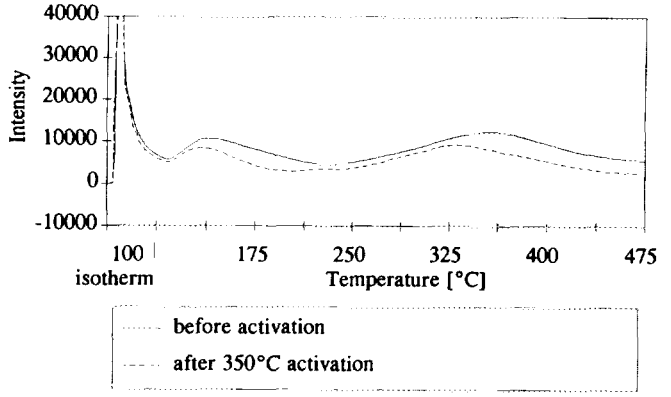

FIG. 7. Ammonia TPD profiles of calcined and activated β-AlF_3 (the respective 5-ml feeds are compared).

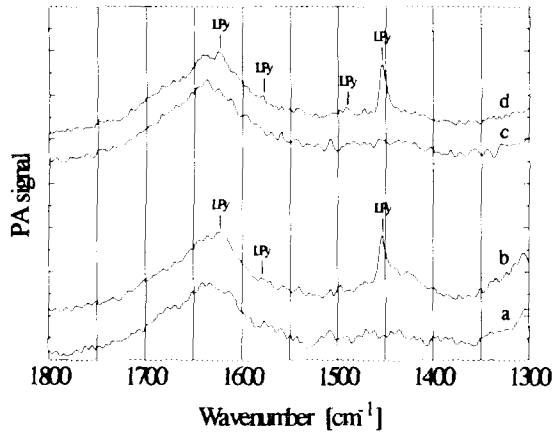

FIG. 8. FTIR photoacoustic spectra of pyridine chemisorbed on modified β-AlF_3 samples: (a) calcined (350°C) (background); (b) calcined (350°C), pyridine adsorption (150°C, 30 μl); (c) activated with $CHClF_2$ (350°C), calcined (350°C) (background); (d) activated with $CHClF_2$ (350°C), calcined (350°C), pyridine adsorption (150°C, 30 μl).

in this behavior. $CHClF_2$ activation was not sufficient for this. This structure remained catalytically inactive.

DISCUSSION

Concerning ammonia desorption intensities and temperatures, there is evidence of a correlation with the behavior of the samples during the activation process. The latter can be divided into two groups of contrary behavior.

Group A is represented by Fig. 10a [$AlF_2(OH)$ activation]. In this figure the course of composition of the haloalkanes is presented as a function of the time of activation (at $t = 0$ a constant $CHClF_2$ flow was set up). At the beginning the solid sample does not exhibit reactivity (no conversion). This corresponds to the ammonia TPD before the activation illustrated in Fig. 6. At the end of activation the sample offers reactivity (approximately 60% conversion of the starting substance). This is accompanied by an increase in ammonia desorption according to Fig. 6 after activation. γ-Al_2O_3 exhibits similar behavior, but the higher activity is reached earlier. Nevertheless, the same effect of ammonia desorption is observed (Fig. 2).

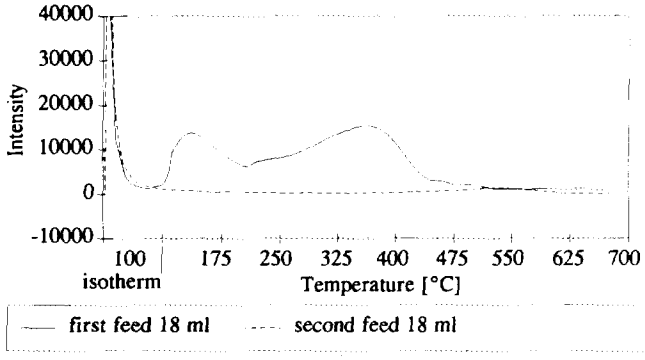

FIG. 9. Ammonia TPD profiles of calcined β-Alf_3 (heated to 700°C) (the second feed represents the properties of the product phase α-AlF_3).

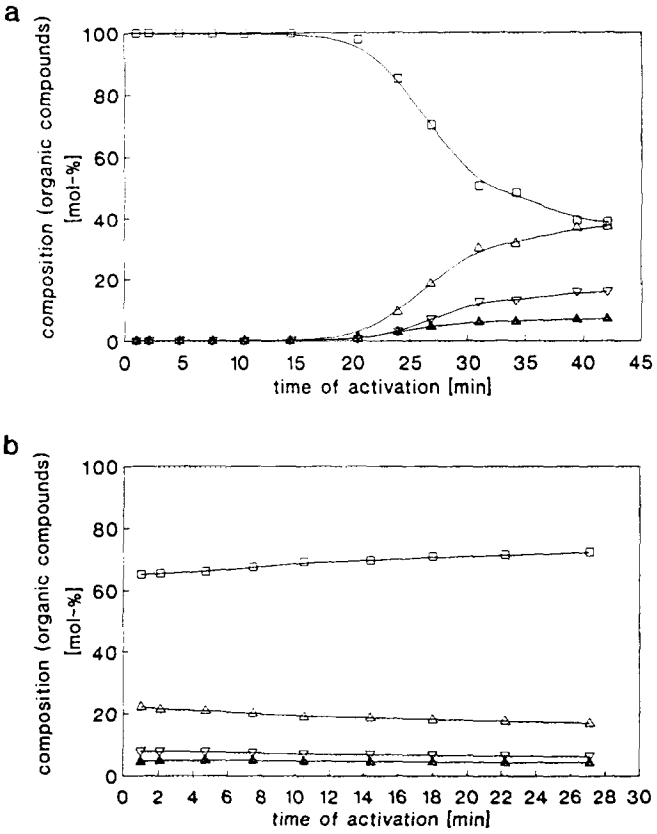

FIG. 10. Change in composition of organic gas phase during activation with $CHClF_2$ (3 liters/h, 350°C, 100 mg catalyst). □,$CHClF_2$; △, CHF_3; ▲, $CHCl_2F$; ▽ $CHCl_3$). (a) $Alf_2(OH)$. (b) β-AlF_3.

On the other hand, Fig. 10b represents the activation behavior of group B. Using β-AlF_3 it is remarkable that there is reactivity from the beginning. According to this behavior, ammonia desorption of the nonactivated sample is not increased by activation (Fig. 7). The slight decrease in conversion with time of activation, as well as the decrease in ammonia desorption, is caused by coke formation and is observed with other samples, too.

α-Cr_2O_3 should be placed between groups A and B. This sample is active after a very short activation. Therefore, there is only a slight increase in ammonia desorption (Fig. 4) after 250°C activation. α-AlF_3 is catalytically inactive and does not adsorb detectable amounts of ammonia or pyridine. For the differences between the structures of α- and β-AlF_3 one may refer to Ref. [1].

Table 2 presents the measured ammonia adsorption in comparison with the respective specific reactivity r_s at the

TABLE 2

Survey Concerning Temperature-Programmed Desorption and Reactivity Data

Sample	Treatment	Second feed: Probe molecule (NH_3) volume (ml)	Amount of desorbed substance: 100–700°C		325–700°C		325–400°C		Specific reactivity (rate/surface): Temperature (°C)	r_s s^{-1}/m^2)
			μmol	μmol/m²	μmol	μmol/m²	μmol	μmol/m²		
γ-Al_2O_3	Before activation	18	397	2.7	106	0.72	60	0.41		
	After 250°C activation	30	928	8.3	652	5.8	205	1.8	250	0.075
	After 400°C activation	18	214	1.9	94	0.84	31	0.27	400	0.16
α-Cr_2O_3	Before activation	5	229	4.7	117	2.4	42	0.86		
	After 250°C activation	5	241	4.9	142	2.9	45	0.92	250	0.023
	After 400°C activation	5	154	3.2	26	0.53	14	0.29	400	0.28
			Amount of desorbed substance: 100–475°C		100–400°C		325–400°C			
			μmol	μmol/m²	μmol	μmol/m²	μmol	μmol/m²		
β-AlF_3	Before activation		264	12.2	195	9.0	69	3.2		
	After 350°C activation	5	163	7.5	140	6.5	49	2.3		
		5							350	0.3
$AlF_2(OH)$	Before activation	5			41	3.9	4	0.38		
	After 350°C activation	5			52	5.0	45	4.3	350	1.0

appropriate temperature (see Experimental). The higher reactivity of γ-alumina at 250°C compared with α-Cr_2O_3 is accompanied by larger amounts of ammonia adsorption per unit surface in all temperature regions (cf. Table 2). The 400°C values show a higher reactivity of α-Cr_2O_3 due to smaller coke formation. It is remarkable that only the temperature regions 100–700 and 325–400°C confirm this effect. The region of the strongest sites (325–700°C) offers a larger ammonia adsorption for γ-alumina having a lower reactivity. This can be explained by the fact that the strongest sites lead to irreversible haloalkane adsorption. The result is failure of the dismutation reaction to occur. Instead, degradation processes with coke formation occur. A further reason is that the ammonia TPD indicates both Lewis and Brønsted acid sites. Brønsted acid sites chemisorb ammonia, but they are not required for the catalysis of dismutation.

Concerning the $AlF_2(OH)$ sample, it can be seen that the higher specific reactivity compared with β-AlF_3 is not accompanied by higher ammonia adsorption in the total temperature range. The observed increase in ammonia adsorption for activated $AlF_2(OH)$ appears in the temperature range 325–400°C, indicating acid sites of a medium strength. The comparison of this medium range results in a correlation between ammonia adsorption and specific reactivity for all samples. Obviously, sites of lower strength (desorption temperatures below 300°C) are not important for the catalysis.

Also, very strong sites probably do not contribute to the catalytic activity. Ammonia TPD of the 250°C activated γ-alumina reveals very strong sites (see Fig. 2), but the comparison between the pyridine adsorption complexes on activated γ-alumina and β-AlF_3 (Fig. 11) does not show stronger Lewis acid sites on γ-alumina (see the discussion about the 19b wavenumber shift in the succeeding paragraphs). Therefore, it can be concluded that the strong acid sites on 250°C activated γ-alumina exhibit Brønsted acidity. Stable ammonium ions were formed on the surface. These strong Brønsted sites may lead to coke formation, but the coke layer deactivates sites of the whole strength distribution.

The desorption temperature range 325–400°C is an arbitrary selection, but the behavior of $AlF_2(OH)$ shows the catalytic unimportance of desorption temperatures below approximately 325°C. High-temperature-activated α-Cr_2O_3 and β-AlF_3 exhibit reactivity without having desorptions at temperatures above approximately 450°C (cf. Figs. 4 and 7). Therefore, the medium desorption temperature range seems to represent the catalytically active sites.

As a result of the pyridine measurements the following conclusion can be drawn. Obviously, the type of the acidity that is important for catalysis of $CHClF_2$ dismutation is Lewis acidity. Brønsted acid sites which appeared on activated γ-alumina are not required for this type of halogen exchange reaction. Nevertheless, Brønsted acidity plays an important role in hydrocarbon oligomerizations, cracking processes, isomerizations, and many other reactions (14, 16, and references therein).

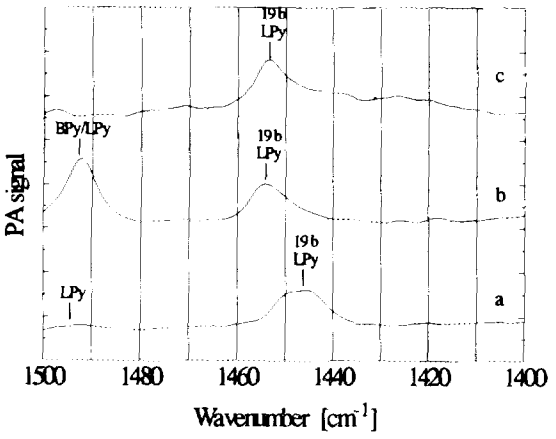

FIG. 11. Shift of the 19b ring mode vibration of pyridine chemisorbed on calcined and activated γ-alumina and calcined β-AlF_3 toward higher wavenumbers: (a) γ-Al_2O_3, calcined (250°C), pyridine adsorption (150°C, 30 μl); (b) γ-Al_2O_3, activated with $CHClF_2$ (250°C), calcined (250°C), pyridine adsorption (150°C, 30 μl); (c) β-AlF_3, calcined (350°C), pyridine adsorption (150°C, 30 μl).

After activation of γ-alumina an increase in the strength of Lewis acid sites is observed. This alteration in strength can be seen in the wavenumber shift of the 19b mode vibration of pyridine chemisorbed on Lewis acid sites (Fig. 11). Due to the inductive effect of fluoride the partial replacement of O and OH by F results in an increase in the Lewis acidity of fluorinated alumina. Afterward, the catalyst is active. As can be seen from Fig. 11, β-AlF_3 already possesses these stronger Lewis sites after calcination. Therefore, it is immediately active and able to catalyze the dismutation.

We believe that aluminum cations of a certain coordination may be identical to these Lewis acid sites. In these circumstances the following reaction pathway can be assumed: The partially positively charged aluminum cations cause a loosening of the C–halogen bond of the haloalkane molecule. This is the first step. In further steps nucleophilic groups attack the positively charged carbon atom. In the case of nucleophilic OH groups, hydrolysis occurs; in the case of a nucleophilic halogen atom of a second haloalkane, a dismutation reaction takes place, and in the case of a nucleophilic attack by halide ions of the solid surface a halogen exchange occurs between the solid surface and the adsorbed haloalkane molecules. All these reactions can be observed depending on the reaction conditions.

ACKNOWLEDGMENTS

Financial support was provided by the Fonds der Chemischen Industrie and by the Deutsche Forschungsgemeinschaft.

REFERENCES

1. Hess, A., and Kemnitz, E., *J. Catal.* **148,** 270 (1994).
2. Kemnitz, E., and Hess, A., *J. Prakt. Chem.* **334,** 591 (1992).
3. Peri, J. B., *J. Phys. Chem.* **69,** 231 (1965).
4. Basila, M. R.,., and Kantner, T. R., *J. Phys. Chem.* **71,** 467 (1967).
5. Knözinger, H., *Adv. Catal.* **25,** 184 (1976).
6. Peri, J. B., *J. Phys. Chem.* **72,** 2917 (1968).
7. Riseman, S. M., Massoth, F. E., Murahli Dhar, G., and Eyring, E. M., *J. Phys. Chem.* **86,** 1760 (1982).
8. Knözinger, H., *Adv. Catal.* **25,** 184 (1976).
9. Kiviat, F. E., and Petrakis, L., *J. Phys. Chem.* **77,** 1232 (1973).
10. Morterra, C., and Cerrato, G., Langmuir **6,** 1810 (1990).
11. Morterra, C., Magnacca, G., Cerrato, G., Del Favero, N., Filippi, F., and Folonari, C. V., *J. Chem. Soc. Faraday Trans.* **89,** 135 (1993).
12. Gil, F. J., Garcia Fierro, J. L., and López Agudo, A., *Z. Phys. Chem.* **123,** 115 (1980).
13. Urban, M. W., and Koenig, J. L., *Appl. Spectrosc.* **40,** 851 (1986).
14. Matulewicz, E. R. A., Kerkhof, F. P. J. M., Moulijn, J. A., and Reitsma, H. J., *J. Colloid Interface Sci.* **77,** 110 (1980).
15. Kline, C. H., and Turkevich, J., *J. Chem. Phys.* **12,** 300 (1944).
16. Kerkhof, F. P. J. M., Oudejans, J. C., Moulijn, J. A., and Matulewicz, E. R. A., *J. Colloid Interface Sci.* **77,** 120 (1980).
17. Hess, A., and Kemnitz, E., *Appl. Catal. A: General* **82,** 247 (1992).
18. Kemnitz, E., Hass, D., and Grimm, B., *Z. Anorg. Alleg. Chem.* **589,** 228 (1990).